Pn wave velocity and anisotropy underneath the central segment of the North-South Seismic Belt in China

Guangbao Du[a,b], Qingju Wu[a], Xuemei Zhang[b,*], Jing He[c], Liye Zou[b], Yangyang Feng[d], Jie Liu[b], Fabio Romanelli[e]

[a] Key Laboratory of Seismic Observation and Geophysical Imaging, Institute of Geophysics, China Earthquake Administration, Beijing 100081, China
[b] China Earthquake Networks Center, Beijing 100045, China
[c] Key Laboratory of Crustal Dynamics, Institute of Crustal Dynamics, China Earthquake Administration, Beijing 100085, China
[d] The Inner Mongolia Autonomous Region Seismological Bureau, Hohhot 010051, China
[e] Department of Mathematics and Geosciences, University of Trieste, Trieste 34127 Italy

A R T I C L E   I N F O

A B S T R A C T

We present a Pn wave velocity and anisotropy model of the central segment of the North-South Seismic Belt in China, where there are numerous stable basins and active faults, making this segment attractive for extensive studies. The model was obtained by a tomographic analysis of 49,973 Pn wave phase readings collected by the China Earthquake Networks Center and temporary stations in Yunnan and Sichuan. The tomographic velocity model shows that the average Pn wave velocity is 8.06 km/s; prominent high-velocity (high-V) anomalies are visible under the Sichuan Basin, the Zoige Basin and the Ordos block, which clearly outline their tectonic margins. A pronounced low-velocity (low-V) zone is observed from the Songpan-Ganzi block to the Chuan-Dian and Daliangshan blocks, suggesting the presence of hot material upwelling. The station delay data show a gradual variation from negative to positive values, possibly reflecting a crustal thickness variation from the southwest to the northeast of the study area. A correlation between the Pn wave anisotropy and the distribution of velocity anomalies is observed: anisotropy is relatively weaker in the high-V anomaly zones beneath stable basins, while it is stronger in the low-V anomaly zones and the high-to-low-V anomaly transition zones. The high-resolution velocity and anisotropy tomographic model that we obtained could also provide a better understanding of the study area seismicity, since the occurrence of strong earthquakes seems to be related to the presence and strength of lateral heterogeneities at the uppermost mantle level.

1. Introduction

The central segment of the North-South Seismic Belt in China is tectonically important as it marks the transition from the Tibetan Plateau to the west and the Yangtze Block to the east (Fig. 1). In this segment there are stable basins, such as the Sichuan and Ordos basins, and active faults, including the Longmenshan, Xianshui River and Anninghe-Xiaojiang faults. The North-South Seismic Belt is one of the most intense seismic zones in China (Zhang, 2008), where many large seismic events occurred in both historic and present-day times, such as the 1654 Lixian (Ms 8.0), 1879 Wenxian (Ms 8.0), 2008 Wenchuan (Ms 8.0), 2013 Lushan (Ms 7.0) and 2017 Jiuzhaigou (Ms 7.0) earthquakes. Therefore, this region has become a key area attracting numerous geoscientists to carry out investigations using various methodological approaches, such as deep seismic sounding (Kan and Lin, 1986; Lin et al., 1993; Yang et al., 2011; Feng et al., 2016), seismic tomography (Lei and Zhou, 2002; Wang et al., 2003a; Wu et al., 2006; Ma et al., 2008; Lei et al., 2009; Guo et al.,2009; Bai et al., 2011; Lei and Zhao, 2016), SKS splitting (Chen et al., 1990; Chang et al., 2006, 2008; Shi et al., 2013), Receiver Function analyses (Xu et al., 2007; Li et al., 2009; He et al., 2014; Wen et al., 2018), and surface GPS observations (Wang et al., 2008, 2009; Zhang et al., 2010; Yang et al., 2013).

In general, Pn phase tomography can achieve a denser ray coverage, thus with a better resolution and accuracy, when compared to seismic analyses that utilize other phases interacting with the uppermost mantle (e.g., Ding et al., 1992; Lei et al., 2014; Gu et al., 2016). Unlike SKS data analysis, which can estimate the vertically integrated anisotropy of the mantle (Hearn, 1996), Pn anisotropy tomography can more precisely reveal the nature of lateral heterogeneities and anisotropy within a limited depth range of the uppermost mantle (Lei et al., 2014;
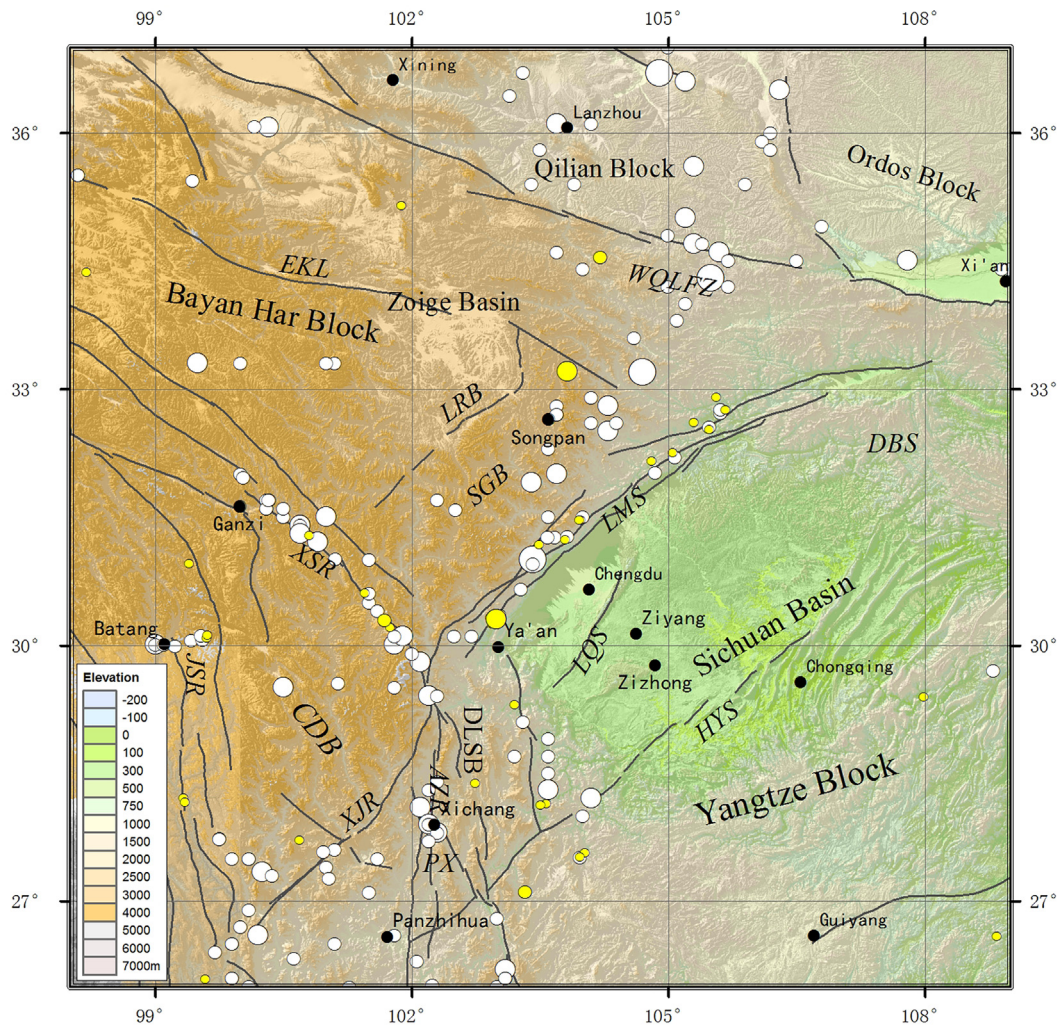
Fig. 1. Map of the study area showing its regional tectonics and the large earthquakes occurred therein. The black lines denote major tectonic features: WQLFZ, Western Qinling fold zone; EKL, Eastern Kunlun fault; LRB, Longriba fault; LMS, Longmenshan fault; XSR, Xianshui River fault; LQS, Longquanshan fault; HYS, Huayingshan fault; XJR, Xiaojin River fault; AZR, Anning-Zemu River fault; JSR, Jinsha River fault; SGB, Songpan-Ganzi block; CDB, Chuan-Dian block; DLSB, Daliangshan block; DBS, Dabashan arcuate tectonic zone; PX, Pan-Xi region. White circles denote the epicenters of the earthquakes, with magnitude larger than 6.0, occurred till 2008; yellow circles denote the epicenters of the earthquakes, with magnitude larger than 5.0, occurred after 12 may 2008; the size of the circles is proportional to the earthquake magnitude. (For interpretation of the references to colour in this figure legend, the reader is referred to the web version of this article.)

Zhou and Lei, 2016). In recent years, many researchers have turned their attention to the velocity and anisotropy structure of the uppermost mantle under the study area (Wang et al., 2003b; Pei et al., 2003; Huang et al., 2003; Liang and Song, 2006; Xu et al., 2010; Li et al., 2011; Li and Lei, 2012; Wang et al., 2013a; Lei et al., 2014; Zhou and Lei, 2016), inferring significant results. Although these results show some similarities in the velocity anomalies and anisotropy patterns, they still show discrepancies in details that may be partly due to the different Pn data sets used. For example, there are significant differences between the Pn wave anisotropic fast wave direction near the Longmenshan fault given by Xu et al. (2010) and those reported by Huang et al. (2003), Li et al. (2011), and Li and Lei (2012). In addition, due to the limited spatial distribution of the seismic stations and the relatively shorter time period of observational data, the final spatial resolutions of the related models are different. For example, Hearn et al. (2004) achieved a 2° × 2° Pn resolution in the velocity distribution in mainland China, while the results of Liang and Song (2006) and Wang et al. (2003b) featured resolutions of 2.5° × 2.5° and 3° × 3°, respectively. Pei et al. (2007) resolved 3° × 3° cells for Pn velocity; Lei et al. (2014) improved the Pn velocity and anisotropy resolutions, achieving a flexible cell size of 1° × 1° in most of their study areas.

In the present study we combine the Pn arrival time data from the observation bulletins of (a) Seismological Report of Chinese Seismic Stations collected from 1996 to 2008, (b) the Observatory Bulletin of China Digital Seismic Network acquired from 2008 to 2018 and (c) temporary seismic stations, in order to obtain a high-resolution aniso-tropic tomographic model; such a model can provide a better under-standing of the deep tectonic environment in the study area and, thus, also a key to study the strong earthquakes produced therein.

2. Data and method

2.1. Observation data

We study the region enclosed by the polygon with geographical coordinates of 98–109°E longitude, 26–37°N latitude (Fig. 1). The data were selected in a larger region obtained extending the above range by 3° outward on all sides (Fig. 2). The data set used in this study is re-presented by the Pn arrival times obtained from the recordings col-lected by (a) Seismological Report of Chinese Seismic Stations from 1996 to 2008, (b) Observatory Bulletin of China Digital Seismic Net-work from 2008 to 2018, (c) 47 temporary seismic stations from the
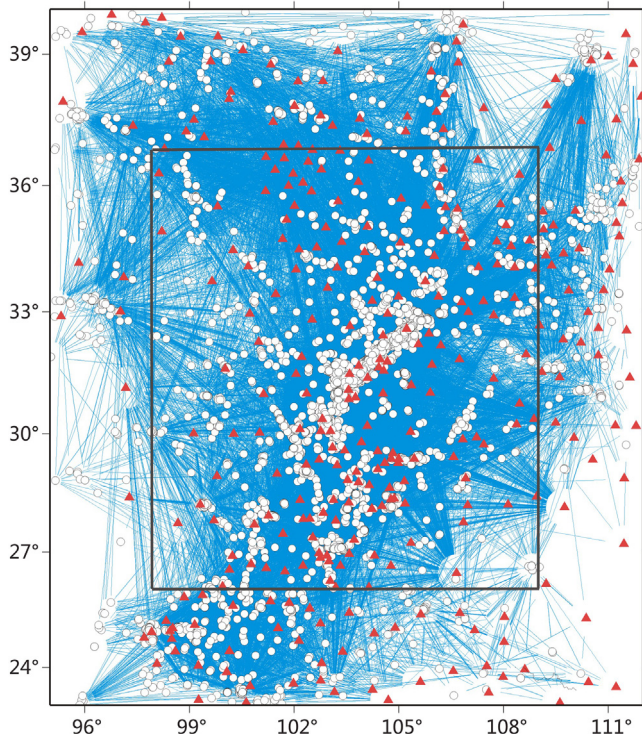
Fig. 2. Geographical distribution of the seismic stations (red triangles), earthquake hypocenters (white circles) and Pn ray paths (blue lines) considered in this study. The gray lines represent the boundary of the study area. (For interpretation of the references to colour in this figure legend, the reader is referred to the web version of this article.)

Yunnan regional seismic network from 2013 to 2015, (d) 30 temporary seismic stations from the Sichuan regional seismic network, and (e) 4 temporary stations installed after the 2017 Jiuzhaigou earthquake.

The following criteria were used to select the Pn data: (1) the epicentral distance is between 2.0° and 15.0°; (2) the focal depth is shallower than 41 km; (3) each event has at least 4 recordings and each station records more than 4 events; (4) the travel time residuals are within ± 4.5 s. The travel time residuals were calculated by subtracting the theoretical values from the observed ones; the theoretical travel times were calculated adopting a mean crust velocity, uppermost mantle velocity and crust thickness of 6.30 km/s, 8.06 km/s and 41 km, respectively. As a result, we obtained 49,973 Pn arrival times from 4405 events recorded by 358 seismic stations whose ray paths are plotted in Fig. 2.

2.2. Method

In this study we adopt the method of Pn anisotropic tomographic technique of Hearn (1996), using Pn travel time residuals to invert for the velocity variations and anisotropy in the uppermost mantle, which is briefly summarized below.

The ray path of the Pn phase can be divided into source, mantle and receiver paths. The source and receiver paths are assumed pertinent to the crust, and their travel times are related to the thickness and velocity of the crust and to the focal depth of the source; the mantle path is assumed to be confined to the uppermost mantle, whose velocity variations, discretized into a set of cells ($0.25° \times 0.25°$, in our case), influence its travel time.

Assuming that Pn velocity is the sum of an average value and a spatially varying perturbation term, the perturbation at any point in space consists of an isotropic component and a certain anisotropic variation. The Pn travel time residual, t_{ij} for the j-th event recorded by the i-th station, can be expressed by the following travel time equation:

$$t_{ij} = a_i + b_j + \sum d_{ijk}(s_k + A_k\cos2\varphi + B_k\sin2\varphi)$$

where φ is the back azimuth angle from event to station, a_i is the static delay of the i-th station, b_j is the static delay of the j-th event, d_{ijk} is the ray length from the j-th event passing through the k-th cell to the i-th station, s_k is the slowness (i.e., reciprocal of velocity) perturbation for the k-th cell, and A_k and B_k are the anisotropic coefficients for the k-th cell. The magnitude of the anisotropy for cell k is given by $\sqrt{A_k^2 + B_k^2}$, whereas the fast direction of Pn propagation is given by $1/2\arctan(B_k/A_k)+90°$ (Pei et al., 2007). The travel time equations involving the unknowns a_i, b_j, s_k, A_k and B_k construct a linear system, which is solved by means of a regularized least squares with a preconditioned version of the LSQR algorithm.

In order to select an optimal pair of damping parameters for the velocity and anisotropy inversion, a number of tests were made by changing their values to form the L-shaped curves (Boschi et al., 2006). The damping parameter is determined at the maximal curvature of the L-shaped curve (Boschi et al., 2006) of Root-Mean-Square (RMS) of travel time residuals versus RMS of velocity perturbation (Fig. 3a). Then, the selected velocity damping factor is fixed and different anisotropic damping factors are utilized to perform the inversion: the optimal value is the one corresponding to the intersection of the trade-off curves between the RMS of velocity and anisotropy perturbations. In our case, the test results provided a value of 100 and 430 as damping factors for velocity and anisotropy, respectively, with a number of iterations equal to 60.

3. Inversion results

The lateral variation and azimuthal anisotropy of Pn wave velocity in the uppermost mantle in the central segment of the South-North
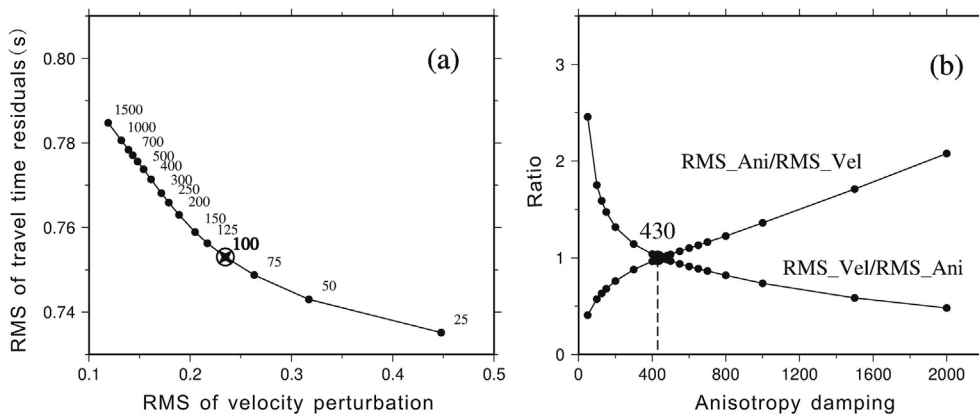
Fig. 3. (a) Trade-off (or L-shaped) curves for RMS (Root-Mean-Square) of travel time residuals versus RMS of velocity perturbation. (b) RMS_Vel/RMS_Ani, the ratio of RMS of velocity perturbations to RMS of anisotropy variations, and RMS_Ani/RMS_Ve, the ratio of RMS of anisotropy variations to RMS of velocity perturbations, are plotted versus anisotropy damping.
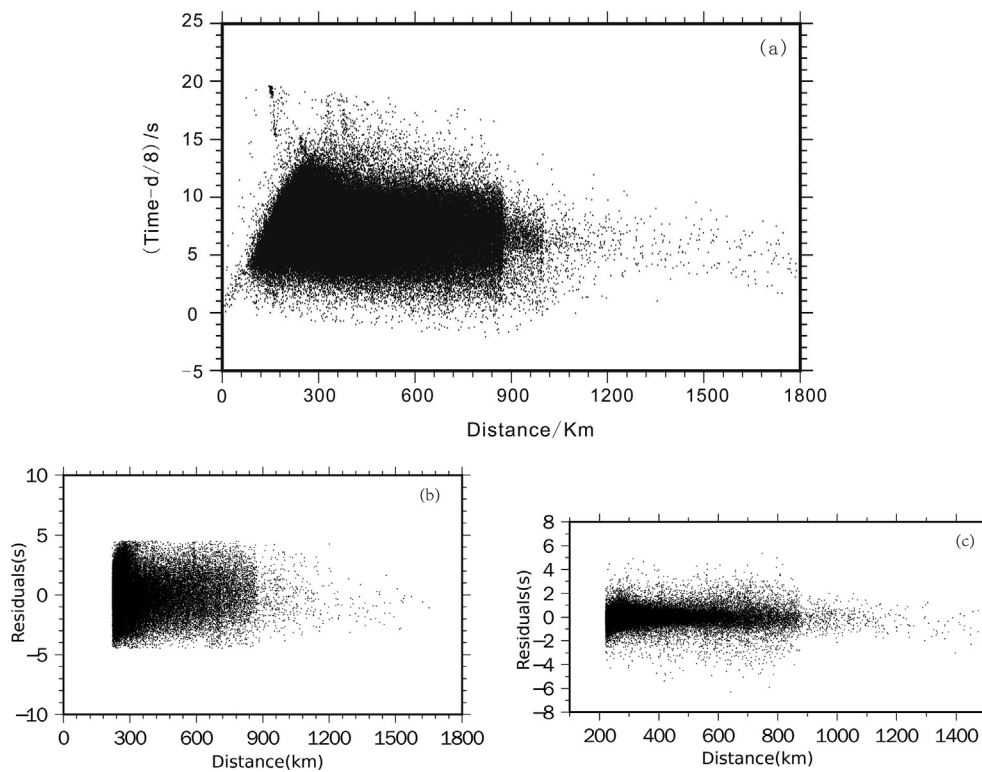
Fig. 4. Distribution of travel time residuals (in s) versus distance (in km). (a) Initial, relative to an average apparent velocity of 8 km/s; (b) before inversion; (c) after inversion.

Seismic Belt were obtained using the method of Pn anisotropic tomographic technique of Hearn (1996), as summarized in Section 2.2. The distribution of travel time residuals initially obtained from our combined data set and relative to an average apparent velocity of 8 km/s (Fig. 4a) is shown in Fig. 4b and c, before and after the inversion, respectively; their standard deviation decreases from 1.77 s to 0.68 s, clearly indicating their convergence after the inversion process.

3.1. Resolution

In order to estimate the effects of the ray coverage on the spatial resolution reachable by our tomographic model and evaluate the reliability of the results, a series of checkerboard tests were applied. A checkerboard test for the Pn velocity model was created by assigning tessellated velocity anomalies with amplitude of ± 0.3 km/s to the reference values of the cells belonging to the considered domain. Synthetic arrival times were calculated for the test model using the same numbers of events, stations, and ray paths as those used for the tomographic inversion of the real data; these synthetic arrival times were then inverted for velocity using the same algorithm adopted for the inversion of real data (Pei, 2002). Then, the spatial resolution is considered to be acceptable for the region in which the checkerboard pattern is recovered. In Fig. 5a and b we display the results of the Pn velocity checkerboard tests: in most of the study areas the spatial resolution reaches $1° \times 1°$ (Fig. 5a), and in some of the central areas the resolution even reaches $0.5° \times 0.5°$ (Fig. 5b). In Fig. 5c we display the results of the Pn anisotropy checkerboard test, showing that the spatial resolution reaches only $1° \times 1°$ in most of the considered areas. This poorer, compared to velocity results, resolution can be explained by the fact that the inversion process involves two more parameters (i.e. A_k and B_k) given the same number of ray paths.

In general, the inversion results obtained in this work are consistent with those from previous Pn wave tomography studies (Wang et al., 2003b; Pei et al., 2003; Huang et al., 2003; Liang and Song, 2006; Xu et al., 2010; Li et al., 2011; Li and Lei, 2012; Wang et al., 2013a; Lei

et al., 2014), also showing a significant improvement in terms of Pn velocity resolution. Based on these results, in the next Sections we discuss in some more detail the Pn wave velocity structure and anisotropy in the uppermost mantle in the central segment of the North-South Seismic Belt (with the exception of adjacent areas), trying also to analyse some deep structural characteristics in this area.

3.2. Pn wave velocity structure of the uppermost mantle

Fig. 6 shows our results for the Pn velocity variations in the uppermost mantle throughout the study area, with perturbations ranging from −0.51 km/s to +0.50 km/s respect to the mean value of 8.06 km/s, evidencing that some lateral heterogeneities are related to surface geological structures and to tectonic features. Both the old and stable Sichuan Basin and the Ordos block show prominent high-velocity (high-V) anomalies, while some weaker high-V anomalies exist around the Zoige Basin and under the western Chuan-Dian block and West Qinling fold zone. A nearly N-S low-velocity (low-V) anomaly zone extends from the Songpan-Ganzi block, where, between the Longmenshan fault and the Longriba fault, velocities can reach a low value of 7.5 km/s, to the Chuan-Dian and Daliangshan blocks. Some small-scale low-V anomalies are visible around the Daba Mountains, the Qilian block and the area on the West of the Zoige Basin.

3.3. Pn wave anisotropy

Fig. 7 shows our results for the Pn anisotropy model, where the lengths of the lines indicate the anisotropy strength and their orientations indicate the fast wave direction that is presumably related to surface structural features. In the Qilian-Qinling fold zone the fast direction of Pn propagation generally varies from EW to SE; it is oriented mainly NW in the Bayan Har block to the west of 99°E, while further eastward it becomes nearly NS to the west of Zoige Basin and then NW; in the Songpan-Ganzi block, on the eastern side of the Longriba fault, it is NE-oriented being parallel to the strike of the Longmenshan fault.
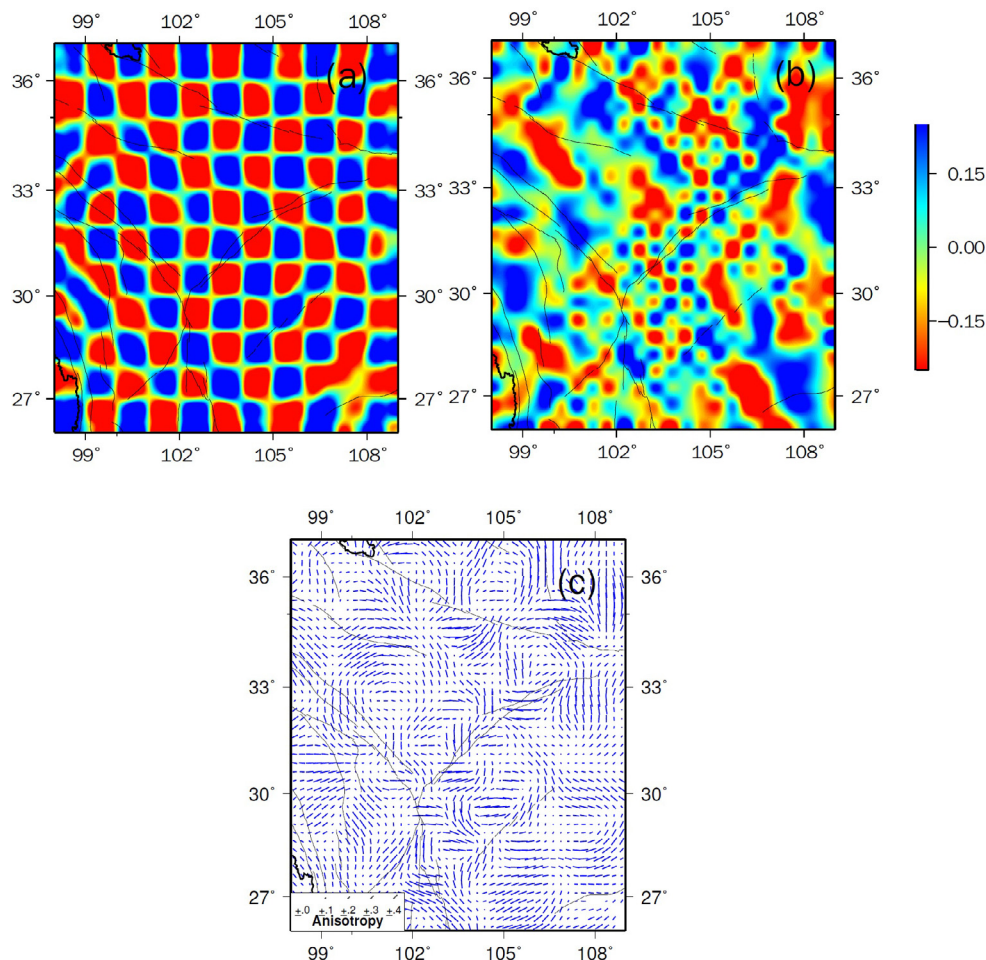
Fig. 5. Checkerboard tests for Pn velocity, with a resolution of 1° × 1° (a) and 0.5° × 0.5° (b), and Pn anisotropy, with a resolution of 1° × 1° (c).

From the western margin of the Chuan-Dian block to 100°E, the fast wave direction is nearly EW; to the east, on the northern side of the Panxi area, the direction is NW, while on the western side of the Panxi area the direction is NS. The Sichuan Basin can be divided into three parts: the fast wave direction is NE in western, EW in central and NS in eastern parts, respectively. In general, the fast directions are generally tangential to the basin margins, along their northern and eastern sides.

3.4. Station delays

The station delays (ranging from −0.7 s to +1.5 s) estimated at the stations considered in this study (from a total of 358 delay data) are shown in Fig. 8. They mainly reflect the variations of crustal velocity and thickness below the locations of the stations: for example, when the mean crustal P wave velocity is 6.3 km/s a station delay of 1.0 s corresponds to a crustal thickness variation of 10.2 km; when the crustal thickness is 50 km a station delay of 1.0 s corresponds to a crustal velocity variation of 0.5 km/s. Considering that the average crustal velocity varies slightly in China, i.e. between 6.2 and 6.5 km/s according to Li and Mooney (1998), if the station delay is larger than 1.0 s it mainly reflects a crustal thickness variation. The average crustal thickness of the study area is 41 km and, based on an adjustment by the delay time of each station multiplied by 10.2, the crustal thickness in the study area varies from 33 km to 56 km. As shown in Fig. 8, most of them (with a few exceptions) show a gradual increase in crustal thickness from East to West and from South to North, reflecting the effect of the obstruction of eastward material flow beneath the Qinghai-Tibet Plateau by the rigid Sichuan Basin (Royden et al., 1997;

Beaumont et al., 2001; Godin et al., 2006; Cao et al., 2009; Yang and Liu, 2009; Zhang et al., 2014).

In order to verify the reliability of our estimates of the crustal thickness beneath the considered stations, our results were compared with those available from previous studies covering the study area and obtained with complementary methodologies. In particular, considering the Receiver Function (RF) method, Lou et al. (2008), Li et al. (2009), Yao et al. (2014) and Zhang et al. (2015a) report the crustal thickness for the Longmenshan fault zone, the Yunnan Province and its neighbouring areas, the West Qinling orogenic belt and the eastern boundary of the Chuan-Dian block, respectively.

The crustal thickness beneath the stations in common between our and the previous mentioned RF studies (for a total of 148 stations) is analysed: the discrepancies in the crustal thickness are less than 5 km in the 77% of the cases (i.e., for 114 stations), and less than 10 km in the 95.3% of the cases (i.e., for 141 stations), showing a very good mutual agreement. In addition, the crustal thickness contour lines obtained by Teng et al. (2013), who used the deep seismic sounding technique, reveal another mutual agreement between findings obtained from complementary approaches (Fig. 8).

4. Discussion

4.1. Comparison with recent Pn tomographic models

Recently, some Pn tomography models were performed in the North-South Seismic Belt and its adjacent areas. Hearn et al. (2004) achieved a 2° × 2° Pn velocity distribution in mainland China, and the
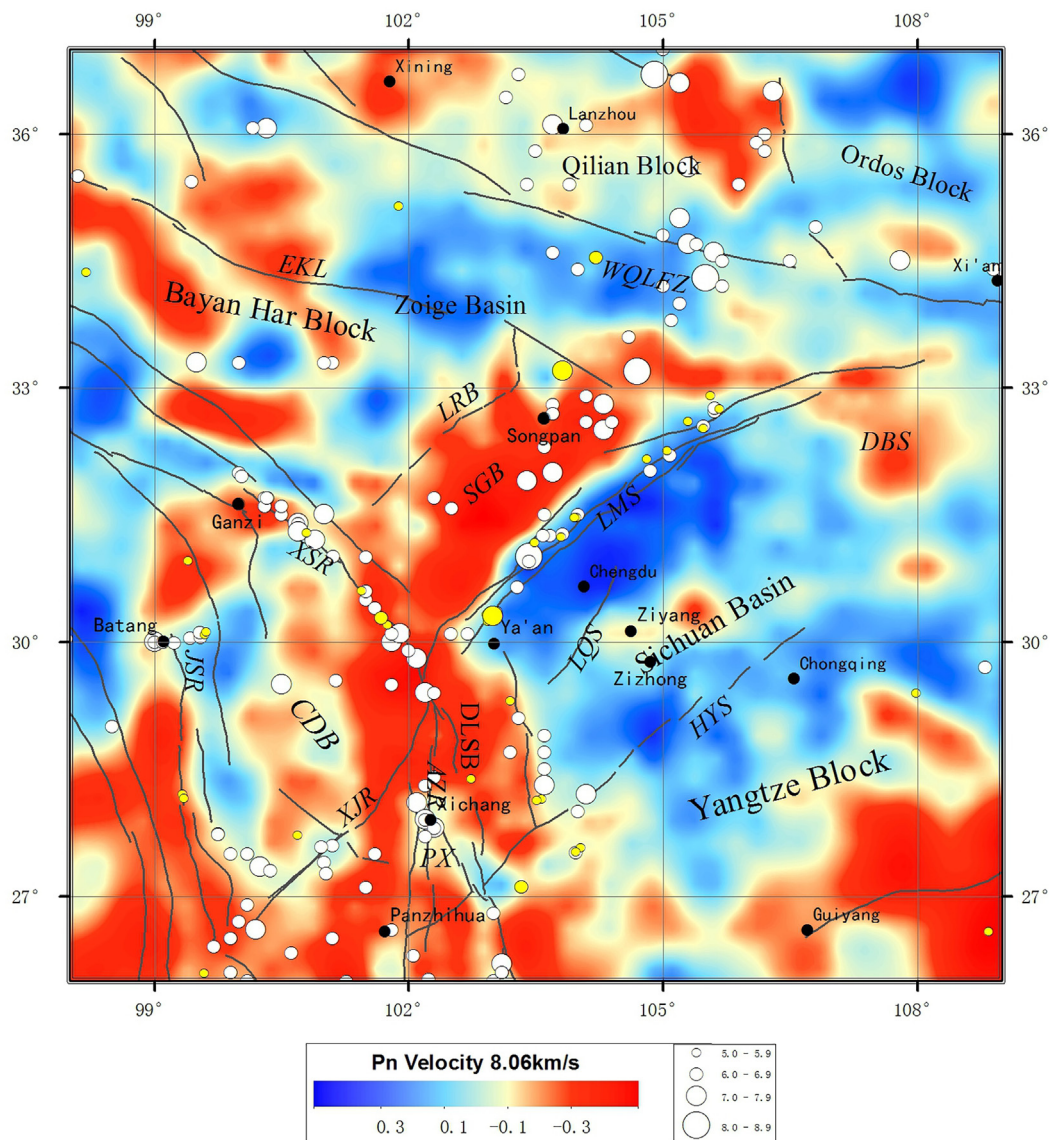
Fig. 6. Map of the study area with Pn-wave velocity (red and blue colors denote low and high velocity anomalies respectively), major tectonic features and epicenters of strong earthquakes (see also the caption to Fig. 1). (For interpretation of the references to colour in this figure legend, the reader is referred to the web version of this article.)

results of Liang and Song (2006) and Wang et al. (2003b) featured resolutions of 2.5° × 2.5° and 3° × 3°, respectively. Pei et al. (2007) resolved 3° × 3° cells for Pn velocity and 4° × 4° cells for anisotropy. Lei et al. (2014) improved the Pn velocity and anisotropy resolutions, achieving a flexible cell size of 1° × 1° in most of their study areas. Compared to these previous studies, we have added new seismic catalogue and phase data, including events relocated using a regional three-dimensional velocity structure, and calculated the Pn velocity with a cell size of 0.5° × 0.5° (Fig. 5) in the Sichuan Basin and its adjacent areas. Recent studies have shown that there is a prominent high-V zone in the Sichuan Basin and, in addition to this stable basin, relatively high velocities are also observed along its margin (Hearn et al., 2004; Liang and Song, 2006; Pei et al., 2007). Lei et al. (2014) presented a model with a clear outline of the Sichuan Basin with a high-V anomaly and a pronounced low-V zone from the Songpan-Ganzi block to the Chuan-Dian block. In our detailed model, the velocities reveal differences in the western, central and eastern portions of the Sichuan Basin. Concerning the anisotropy features, the Pn fast direction has not been clearly revealed in the central segment of North-South Seismic Belt by previous models (Liang and Song, 2006; Wang et al., 2003b). Hearn

et al. (2004) have not provided the Pn anisotropy, while the fast direction is approximately E-W in the Sichuan Basin (Pei et al., 2007). In our model, the Pn fast direction pattern (see Fig. 8), is consistent with the configuration of the main tectonic blocks.

4.2. Pn velocity variation

Velocity variations in the uppermost mantle can be the effect of changes in temperature, pressure, composition, anisotropy, water presence and volatile content. Among these possible factors, temperature is the most important one, with compositional variations due to presence of water as the possible secondary one (Hearn, 1984, 1996; Hearn et al., 2004). Stable blocks, such as the Sichuan Basin and the Ordos block, show high-V anomalies in the uppermost mantle (Fig. 6), which are consistent with the results of previous studies (Huang et al., 2003; Li et al., 2011; Li and Lei, 2012; Liang and Song, 2006; Xu et al., 2010; Wang et al., 2013a). In addition, our results show stronger high-V anomalies under the basins, with their shapes much better coupled with these tectonic margins.

Although most parts of the Sichuan Basin are characterized by a
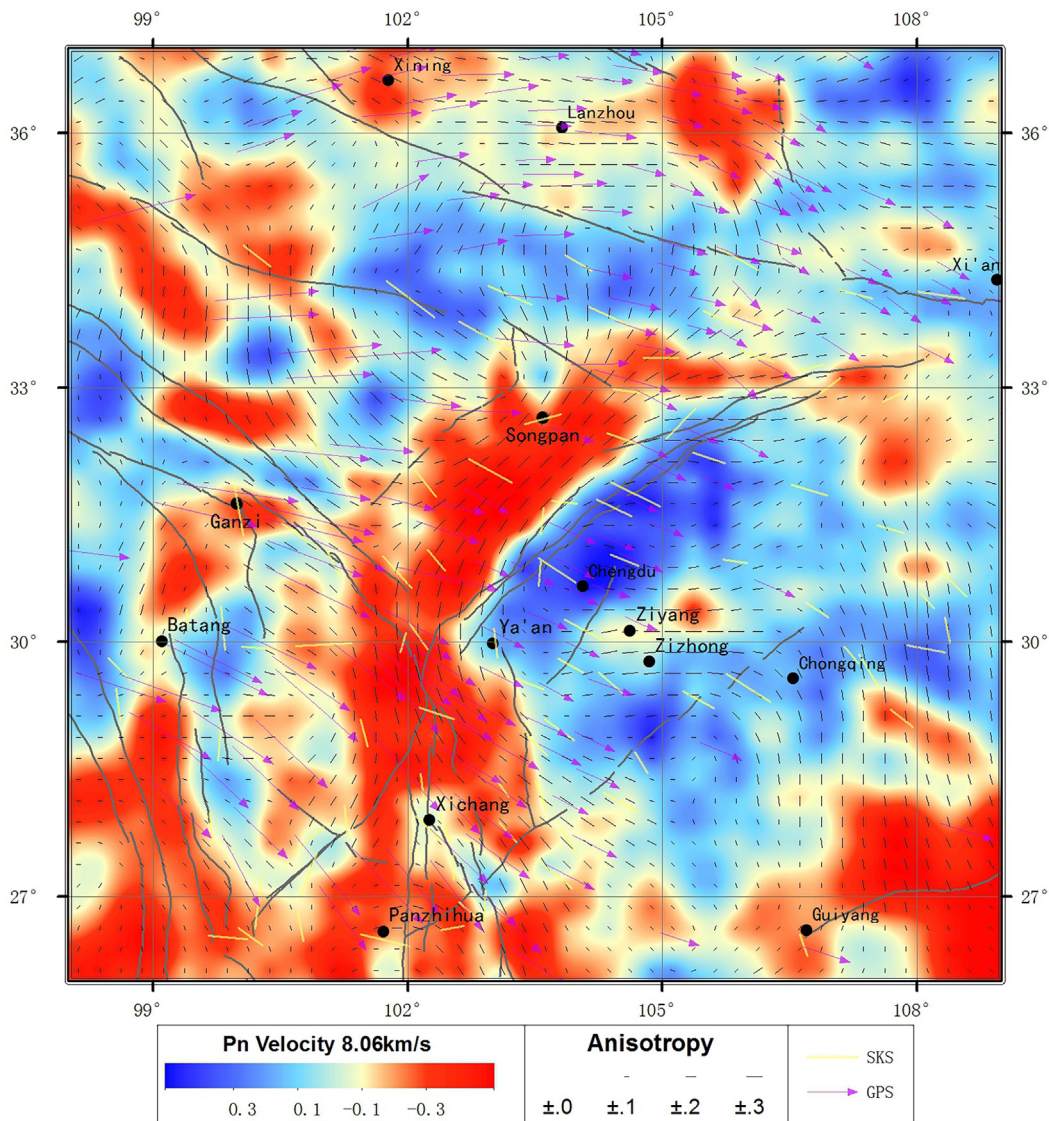
Fig. 7. Map of the study area with the tomographic image of Pn velocity and anisotropy. Black line segments are drawn parallel to the direction of fast Pn velocity, with their length proportional to the magnitude of anisotropy (Chang et al., 2008); yellow line segments indicate SKS fast direction; purple arrows represent the GPS velocity field relative to the stable Eurasia (Gan et al., 2007). (For interpretation of the references to colour in this figure legend, the reader is referred to the web version of this article.)

high-V anomaly, a relatively low-V zone is observed in the center of the basin (Fig. 6). Guo et al. (1996) propose that the Longquanshan and Huayingshan faults divide the Sichuan Basin into three parts: western, central and eastern Sichuan Basin. Asthenospheric upwelling occurs in central Sichuan due to isostatic gravitational processes, resulting in a high mantle heat flow of 35.73 mW/m² in this region where the temperature at the Moho is 863 °C (Guo et al., 1996); these values are much higher than those in the eastern and western Sichuan regions. Geothermal heat flow, reflecting the thermal state and structure of the lithosphere, may have an intrinsic relationship with Pn wave velocity (Huang and Wang, 1992); thus, high heat flow values may explain why the velocity in the uplifted area of central Sichuan is lower than the velocities in adjacent regions. High-V anomalies under Zoige Basin are detected in the present study, a feature that is supported also by deep seismic soundings (Jia et al., 2009); in addition, an investigation of magnetotelluric imaging (Wang et al., 2013b) shows a large number of high-resistivity blocks from the lower crust to the uppermost mantle beneath this basin. These evidences and the earthquake distribution within the Zoige Basin, where no large historical earthquakes have

occurred, indicate that this area is relatively stable.

A nearly NS low-V anomaly zone extends from the Songpan-Ganzi block, along the Xiaojinhe fault, to the Chuan-Dian and the Daliangshan blocks (Fig. 6). At a depth of 40 km, a low-V zone is observed in the lower crust from the Songpan-Ganzi block to the Longmenshan fault (Liu et al., 2018). The tectonic activity is intense in this area, which separates the Qinghai-Tibet Plateau and the Yangtze Platform. Thermal upwelling in the mantle may exist beneath this area, and this hypothesis is consistent with previous research results (Huang et al., 2003; Liang and Song, 2006; Xu et al., 2010; Li et al., 2011; Li and Lei, 2012; Wang et al., 2013a; Lü et al., 2017). The deep seismic soundings deployed by Wang et al. (2003a) from Batang to Zizhong show that the average Pn wave velocity in this region is 7.7–7.8 km/s. Our study obtains consistent results along this profile, providing more details about velocity structure that are also supported by magnetotelluric imaging (Zhang et al., 2012).

A weak high-V zone is revealed in the Panxi area between Xichang and Panzhihua, and the velocity therein is close to the average velocity (8.06 km/s) of the study area. A geomagnetic study (Ren and Yan,
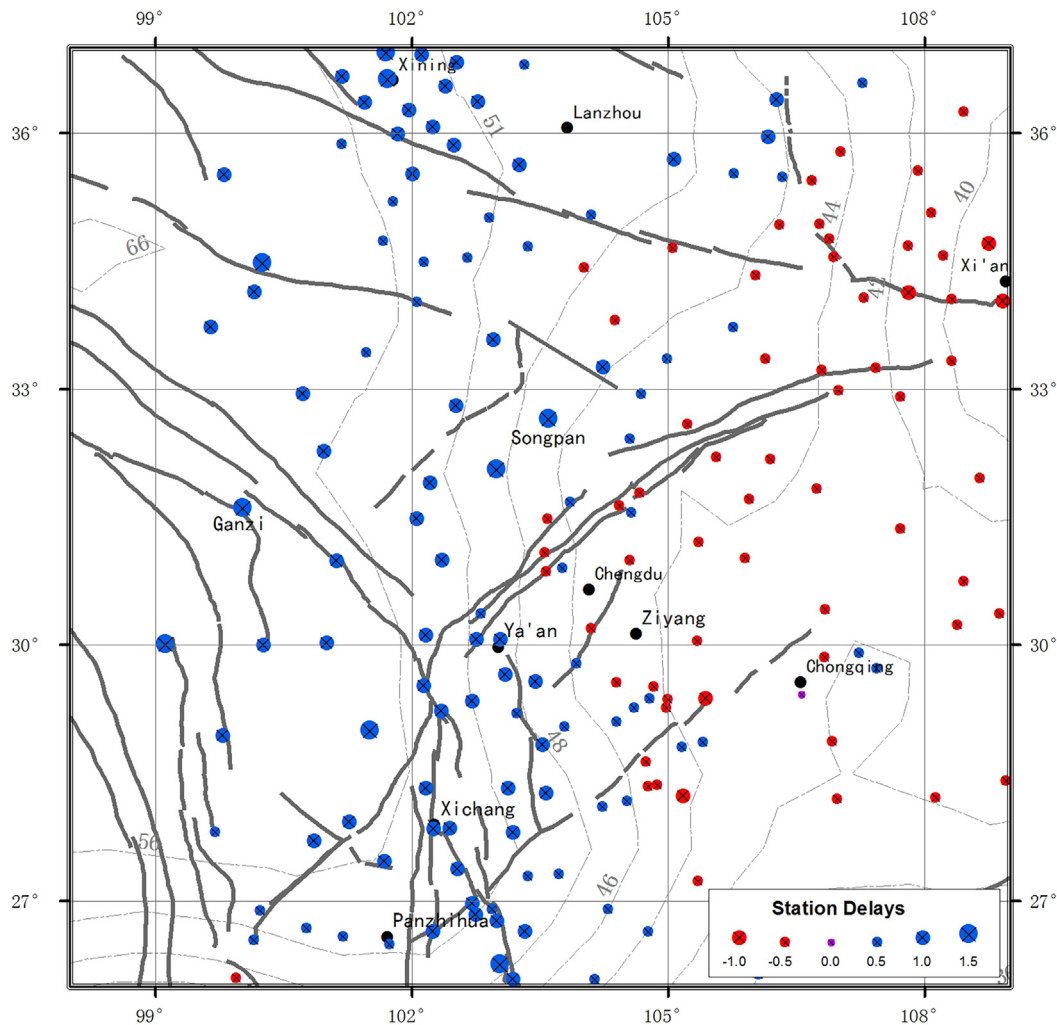
Fig. 8. Map of the study area with the station delays for Pn travel times. The "×" symbols indicate stations locations, with circles denoting negative (red) or positive (blue) delays in seconds; the thin lines represent Moho depth contours, with numbers denoting the depth values in km (Teng et al., 2013). (For interpretation of the references to colour in this figure legend, the reader is referred to the web version of this article.)

1987) demonstrated that the Panxi area displays an isolated positive anomaly surrounded by a negative anomaly. From a conductivity perspective, thick high-resistivity bodies are distributed throughout the area; the surface geology indicates that these high-resistivity bodies may reflect basic to basic-ultrabasic magmatic complex and deep metamorphic granulite (Zhang et al., 2015b). According to the distribution of historical seismicity (Fig. 6), no earthquakes with magnitudes larger than 6 have occurred in this region. Overall, the Panxi area is stable and features a high resistivity and a high velocity: it may be the place of a channel of ancient upwelling magma that subsequently cooled.

4.3. Pn anisotropy

The uppermost mantle anisotropy is generally accepted to be associated with the preferred alignment of olivine crystals due to creep of material in the uppermost mantle, which reflects the trace of the past tectonic deformation (Silver and Chan, 1988, 1991; Hearn, 1996). Therefore, it is of great significance to obtain a reliable uppermost mantle anisotropy image for a better understanding of the plate deformation. For stable continental areas, anisotropy is considered to represent "fossil" anisotropy imprinted within the lithosphere by the most recent large-scale tectonic activity in the area; for continental regions characterized by active tectonism, the anisotropy reflects this ongoing process (Chang et al., 2008). Therefore, this study analyses the

anisotropic characteristics of the study area while incorporating surface GPS observations (purple arrows in Fig. 7) and SKS splitting (yellow lines in Fig. 7).

4.3.1. Qilian block

The fast direction of Pn propagation in the uppermost mantle along the northern margin of the western Qinling fold zone is mainly EW (Fig. 7) and it reorients to the NW on the western side of the Ordos block; these results are similar to those obtained by Lei et al. (2014), being generally consistent with SKS splitting results (Chang et al., 2016) and surface GPS observations (Gan et al., 2007). Considering the counterclockwise rotation of the Ordos block and the associated left-lateral strike-slip faults (Zhang et al., 1998; Teng et al., 2010; Tian et al., 2011; Sun and Kennett, 2016), it is speculated that during the eastward movement of the uppermost mantle material associated with the Qinghai-Tibet Plateau encountered the Ordos block and changed direction, turning southward around the Ordos block and escaping eastward between the rigid Ordos block and the Sichuan Basin.

4.3.2. Bayan Har block

The fast direction of Pn propagation is quite different from west to east in the Bayan Har block (Fig. 7): the orientation is originally NW and then transitions to the NE and SE in the Zoige Basin; the SE branch changes to a NE orientation in the Songpan-Ganzi block, which is

consistent with the results of previous studies (Huang et al., 2003; Liang and Song, 2006; Li et al., 2011; Li and Lei, 2012; Wang et al., 2013a; Lei et al., 2014). It has been suggested that when the southeastward mantle material flow of Qinghai-Tibet Plateau encountered Zoige Basin it was divided into two branches, one along the NE direction and the other along the SE direction. The SE branch diverges again when it encounters the Sichuan Basin at the margin of the Songpan-Ganzi block: one branch is directed toward the SE, while the other is directed toward the NE and escapes eastward between the Sichuan Basin and the Ordos block. However, there are no significant variations in surface GPS observations (Gan et al., 2007) or SKS splitting results (Chang et al., 2008) indicating that this variation may exist only within a certain depth range in the uppermost mantle.

4.3.3. Chuan-Dian block and Daliangshan block

The fast direction of Pn propagation shows clear differences from Chuan-Dian to Daliangshan blocks: the first shows an approximate EW oriented Pn fast direction and weak high-V anomalies, whereas the second shows NS Pn fast direction and low-V anomalies (Fig. 7). Also if some detailed features that emerge from this picture are different from previous results (Li et al., 2011; Li and Lei, 2012; Lei et al., 2014) the overall pattern is similar, suggesting the existence of hot material upwelling there. More specifically, the fast direction is divided into two branches in the Panxi area. The orientation on the eastern side is NNW, consistent with GPS observations (Gan et al., 2007) and SKS splitting results (Chang et al., 2008), which may suggest a coupling between the crust and the lithospheric mantle in this region. In contrast, the orientation on the western side is NNE, consistent with SKS splitting results (Chang et al., 2008) but different from GPS observations (Gan et al., 2007), indicates the possibility that in this area the uppermost mantle and crust are decoupled. The velocity structure shows that the Panxi area has a weak high-V anomaly: this may indicate the presence of rigid materials that obstruct the flow of plateau material as it flows toward the SE, causing it to diverge.

4.3.4. Longmenshan fault zone and Sichuan Basin

The fast direction of Pn propagation is quite different across the Longmenshan fault zone (Fig. 7): on the western side (beneath the Songpan-Ganzi block) it is approximately oriented in a NE direction, while on the eastern side (beneath the Sichuan Basin) its orientations can be used to individuate three regions, revealing some differences from previous results (e.g. Huang et al., 2003; Liang and Song, 2006; Xu et al., 2010; Li et al., 2011; Li and Lei, 2012; Lei et al., 2014). The western part of the Sichuan Basin shows a significant high-V anomaly and the fast direction is along NS direction in the south and along NE in the northern part, parallel to the Longmenshan fault. The central part of the Sichuan Basin displays a weak high-V anomaly and the anisotropic fast direction is directed EW. In contrast, the eastern part of the Sichuan Basin shows a strong high-V anomaly and the fast wave direction is mainly oriented along NS. Previous studies have revealed that the Sichuan Basin contains different basement compositions (Guo et al., 1996; Zhang et al., 2006), as supported by gravity anomaly results (Xiong et al., 2015). However, the results of surface GPS observations (Gan et al., 2007) and SKS splitting (Chang et al., 2008) do not show significant variations across the Longmenshan fault zone, suggesting a certain degree of decoupling between the lithosphere and the uppermost mantle.

4.4. Relationship between the Pn wave velocity and anisotropy

Fig. 7 shows that the anisotropy strength is associated with velocity anomalies: the high-V areas, such as Sichuan Basin, show weaker anisotropy indicating that they may suffer less deformation; the low-V areas, such as the Songpan-Ganzi, Chuan-Dian and Daliangshan blocks and the Dabashan arcuate tectonic zone, show stronger anisotropy, which may be related to the strong tectonic deformation. Furthermore,

the narrow areas between two high-V anomalies, such as the northeastern part of the Songpan-Ganzi block, between the Sichuan Basin and the Ordos block, and the southeastern part of the Daliangshan block, between the Sichuan Basin and the Panxi area, show strong anisotropy, suggesting that the material flow tends to accelerate when moving through a narrowing passage.

4.5. Pn wave velocity and earthquake distribution

In Fig. 6 the white and yellow circles denote earthquakes: the white circles represent earthquakes (M > 6.0) occurred till 2008, and the yellow circles represent events (M > 5.0) occurred from 2008 to 2018. It is visible that most of the large earthquakes occurred at the transition zones from high-V to low-V anomalies, such as the Songpan-Ganzi block and Sichuan Basin; on the other hand, some earthquakes occurred on the margins of high-V anomalies. These results may suggest that strong earthquakes are prone to occur on boundaries where it is easy to accumulate elastic energy. Most of the aftershocks (M > 5.0) after the 2008 Wenchuan Earthquake (*Ms* 8.0) occurred at the northeastern portion of the Longmenshan fault zone (Fig. 6). The 2013 Lushan earthquake (*Ms* 7.0) has been the only strong earthquake occurred in the Longmenshan fault zone (at its southwestern portion) since the 2008 Wenchuan earthquake: Chen et al. (2013) inferred that there could exist a future seismic risk in the gap between Lushan and Wenchuan aftershocks.

5. Conclusions

In this study we present a high-resolution Pn velocity and anisotropy tomographic model of the uppermost mantle beneath the central segment of North-South Seismic Belt in China. Pn arrival time data set is built from the collection of events recorded by the Seismological Report of Chinese Seismic Stations (from 1996 to 2008), Observatory Bulletin of China Digital Seismic Network (from 2009 to 2018), and temporary seismic stations. Using the Pn velocity inversion method the spatial resolution of the velocity model has significantly improved compared to previous studies, reaching a level up to 0.5° × 0.5° in most of the study area.

The Pn velocity variations show a correlation with tectonic activity: our current model clearly outlines, with high-V anomalies, the Sichuan Basin, Zoige Basin and Ordos block, suggesting that these regions could be stable; there is a weaker high-V anomaly in the Panxi region, suggesting that it may be a channel of ancient upwelling magma that subsequently cooled; an evident low-V anomaly zone is observed from the Songpan-Ganzi block to Chuan-Dian and Daliangshan blocks, suggesting the presence of hot upwelling material; a relatively low-V anomaly is observed in the central region of the Sichuan Basin, suggesting the existence of asthenospheric upwelling there.

The anisotropy strength is associated with velocity anomalies: high-V areas have weaker anisotropy while low-V area shows stronger anisotropy, and the reason may be related to the tectonic deformation. The narrow areas between two high-V anomalies show strong anisotropy, suggesting that the material flow tends to accelerate when moving through a narrowing passage. The strong earthquakes occurred at the high-to-low-V boundaries and on the margins of high-V anomalies, suggesting that the crustal earthquakes could be related to the presence of lateral heterogeneities in the mantle. The fast direction of Pn propagation seems to rotate around stable blocks, like Sichuan Basin and Ordos block, appearing tangential to their boundaries.

Declaration of Competing Interest

The authors declared that there is no conflict of interest.

Acknowledgments

References

Bai, Z.M., Tian, X.B., Tian, Y., 2011. Upper mantle P-wave tomography across the Longmenshan fault belt from passive-source seismic observations along Aba-Longquanshan profile. J. Asian Earth Sci. 40, 873–882.

Beaumont, C., Jamieson, R.A., Nguyen, M.H., Lee, B., 2001. Midcrustal channel flow in large hot orogens: results from coupled thermal-mechanical models. In: Cook, F., Erdmer, P. (Eds.), Slave - Northern Cordillera Lithospheric Evolution (SNORCLE) and Cordilleran Tectonics WorkshopReport of 2001 Combined Meeting, Lithoprobe Rep. 79. Lithoprobe Secretariat, University of British Columbia, Vancouver, pp. 112–170.

Boschi, L., Becker, T.W., Soldati, G., Dziewonski, A.M., 2006. On the relevance of Born theory in global seismic tomography. Geophys. Res. Lett. 33 (6). https://doi.org/10.1029/2005gl025063.

Cao, J.L., Shi, Y.L., Zhang, H., Wang, H., 2009. Numerical simulation of GPS observed clockwise rotation around the eastern Himalayan syntax in the Tibetan Plateau. Chin. Sci. Bull. 54 (8), 1398–1410. https://doi.org/10.1007/s11434-008-0588-7.

Chang, L.J., Wang, C.Y., Ding, Z.F., 2006. A study on SKS splitting beneath the Yunnan region. Chinese J. Geophys. 49 (1), 197–204 (in Chinese with English abstract).

Chang, L.J., Wang, C.Y., Ding, Z.F., 2008. Study on seismic anisotropy of upper mantle beneath the Sichuan and its adjacent areas. Sci. China Ser. D, Earth Sci. 38 (12), 1589–1599 (in Chinese).

Chang, L.J., Ding, Z.F., Wang, C.Y., 2016. Upper mantle anisotropy beneath the northern segment of the north-south tectonic belt in China. Chinese J. Geophys. 59 (11), 4035–4047. https://doi.org/10.6038/cjg20161109 (in Chinese with English abstract).

Chen, P.S., Liu, F.T., Li, Q., Qin, J.Z., 1990. Lateral heterogeneity of velocity structure beneath Yunnan region. Sci. China Ser. D, Earth Sci. 4, 431–438 (in Chinese).

Chen, Y.T., Yang, Z.X., Zhang, Y., Liu, C., 2013. From 2008 Wenchuan earthquake to 2013 Lushan earthquake. Sci. Sin. Terrae 43, 1064–1072 (in Chinese).

Ding, Z.F., Zeng, R.S., Wu, D.M., 1992. The Pn wave velocities and the relief of Moho in the Tibetan Plateau. Acta Seismol. Sin. 11 (S1), 592–599 (in Chinese).

Feng, Y.Y., Yu, C.Q., Fan, Z.G., Song, L.R., Liang, S.S., He, J.J., Mei, Z.F., 2016. Fine crustal structure of the Lushan area derived from seismic reflection profiling. Chinese J. Geophys. 59 (9), 3248–3259. https://doi.org/10.6038/cjg20160910 (in Chinese with English abstract).

Gan, W.J., Zhang, P.Z., Shen, Z.K., Niu, Z.J., Wang, M., Wan, Y.G., Zhou, D.M., Cheng, J., 2007. Present-day crustal motion within the Tibetan Plateau inferred from GPS measurements. J. Geophys. Res. 112 (B8). https://doi.org/10.1029/2005jb004120.

Godin, L., Grujic, D., Law, R.D., Searle, M.P., 2006. Channel flow, ductile extrusion and exhumation in continental collision zones: an introduction. Geol. Soc. Lond. Spec. Publ. 268 (1), 1–23. https://doi.org/10.1144/GSL.SP.2006.268.01.01.

Gu, Q.P., Ding, Z.F., Kang, Q.Q., Zhao, Q.G., 2016. Pn wave velocity and anisotropy in the middle-southern segment of the Tan-Lu fault zone and adjacent region. Chinese J. Geophys. 59 (2), 504–515 (in Chinese with English abstract).

Guo, B., Liu, Q.Y., Chen, J.H., Liu, L.S., Li, S.C., Li, Y., Wang, J., Qi, S.H., 2009. Teleseismic P-wave tomography of the crust and upper mantle in Longmenshan area, west Sichuan. Chinese J. Geophys. 52 (2), 346–355 (in Chinese with English abstract).

Guo, Z.W., Deng, K.L., Han, Y.H., 1996. The Formation and Development of Sichuan Basin. Geological Publishing House, Beijing.

He, C.S., Dong, S.W., Santosh, M., Chen, X.H., 2014. Seismic structure of the Longmenshan area in SW China inferred from receiver function analysis: Implications for future large earthquakes. J. Asian Earth Sci. 96, 226–236.

Hearn, T.M., 1984. Pn travel times in southern California. J. Geophys. Res.: Solid Earth 89 (B3), 1843–1855. https://doi.org/10.1029/jb089ib03p01843.

Hearn, T.M., 1996. Anisotropic Pn tomography in the western United States. J. Geophys. Res.: Solid Earth 101 (B4), 8403–8414. https://doi.org/10.1029/96jb00114.

Hearn, T.M., Wang, S., Ni, J.F., Xu, Z., Yu, Y., Zhang, X., 2004. Uppermost mantle velocities beneath China and surrounding regions. J. Geophys. Res.: Solid Earth 109 (B11). https://doi.org/10.1029/2003jb002874.

Huang, S.P., Wang, J.Y., 1992. The Geothermal and Pn velocity perturbation in the continental area of China. Acta Seismol. Sin. 14 (1), 42–50 (in Chinese).

Huang, J.L., Song, X.D., Wang, S.Y., 2003. Fine structure of Pn velocity beneath Sichuan-Yunnan region. Sci. China Ser. D, Earth Sci. 33 (Suppl.), 144–150 (in Chinese).

Jia, S.X., Zhang, X., Zhao, J.R., Wang, F.Y., Zhang, C.K., Xu, Z.F., Yang, Z.X., Pan, J.S., Liu, Z., Pan, S.Z., Sun, G.W., 2009. Deep seismic sounding data reveal the crustal structures beneath Zoigê basin and its surrounding folded orogenic belts. Sci. China, Earth Sci. 53 (2), 203–212. https://doi.org/10.1007/s11430-009-0166-0. (in Chinese).

Kan, R.J., Lin, Z.Y., 1986. A preliminary study on crustal and upper mantle structure in Yunnan. Earthq. Res. China. 2 (4), 50–61 (in Chinese with English abstract).

Lei, J.S., Zhou, H.L., 2002. 3-D velocity structure of P wave in the upper mantle beneath southwestern China and its adjacent areas. Acta Seismol. Sin. 24 (2), 126–134 (in Chinese with English abstract).

Lei, J.S., Zhao, D.P., Su, J.R., Zhang, G.W., Li, F., 2009. Fine seismic structure under the Longmenshan fault zone and the mechanism of the large Wenchuan earthquake. Chinese J. Geophys. 52 (2), 339–345 (in Chinese with English abstract).

Lei, J.S., Li, Y., Xie, F.R., Teng, J.W., Zhang, G.W., Sun, C.Q., Zha, X.H., 2014. Pn anisotropic tomography and dynamics under eastern Tibetan plateau. J. Geophys. Res. Solid Earth 119, 2174–2198. https://doi.org/10.1002/2013JB010847.

Lei, J.S., Zhao, D.P., 2016. Teleseismic P-wave tomography and mantle dynamics beneath Eastern Tibet. Geochem. Geophys. Geosyst. 17, 1861–1884.

Li, F., Zhou, S.Y., Su, Y.J., Li, P., Deng, C.H., Li, L., Wang, L.L., 2011. Study on Pn-wave velocity structure and anisotropy in the Sichuan-Yunnan and its adjacent areas. Chinese J. Geophys. 54 (1), 44–54 (in Chinese with English abstract).

Li, S.L., Mooney, W.D., 1998. Crustal structure of China from deep seismic sounding profiles. Tectonophysics 288, 105–113.

Li, Y., Lei, J.S., 2012. Velocity and anisotropy structure of the uppermost mantle under the eastern Tibetan plateau inferred from Pn tomography. Chinese J. Geophys. 55 (11), 3615–3624 (in Chinese with English abstract).

Li, Y.H., Wu, Q.J., Tian, X.B., Zhang, R.Q., Pan, J.T., Zeng, R.S., 2009. Crustal structure in the Yunnan region determined by modeling receiver functions. Chinese J. Geophys. 52 (1), 67–80 (in Chinese with English abstract).

Liang, C.T., Song, X.D., 2006. A low velocity belt beneath northern and eastern Tibetan Plateau from Pn tomography. Geophys. Res. Lett. 33 (L22306), 1–5. https://doi.org/10.1029/2006gl027926.

Lin, Z.Y., Hu, H.X., Zhang, W.B., Zhang, H.F., He, Z.Q., Lin, Z.M., Qiu, T.X., 1993. A study on velocity structure of the crust and upper mantle in western Yunnan region. Acta Seismol. Sin. 15 (4), 427–440 (in Chinese).

Liu, Z.Q., Liang, C.T., Hua, Q., Li, Y., Yang, Y.H., He, F.J., Fang, L.H., 2018. The seismic potential in the seismic gap between the Wenchuan and Lushan earthquakes revealed by the joint inversion of receiver functions and ambient noise data. Tectonics 37, 4226–4238. https://doi.org/10.1029/2018TC005151.

Lou, H., Wang, C.Y., Lü, Z.Y., Yao, Z.X., Dai, S.G., You, H.C., 2008. Deep structural environment of 2008 Wenchuan $M_S8.0$ earthquake: Joint interpretation from teleseismic P-wave receiver function and Bouguer gravity anomaly. Sci. China Ser. D, Earth Sci. 38 (10), 1207–1220 (in Chinese).

Lü, Y., Ni, S.D., Chen, L., Chen, Q.F., 2017. Pn tomography with Moho depth correction from eastern Europe to western China. J. Geophys. Res.: Solid Earth 122, 1284–1301. https://doi.org/10.1002/2016JB013052.

Ma, H.S., Zhang, G.M., Wen, X.Z., Zhou, L.Q., Shao, Z.G., 2008. 3-D P wave velocity structure tomographic inversion and its tectonic interpretation in southwest China. Earth Sci. J. China Uni. Geosci. 33 (5), 591–602 (in Chinese with English abstract).

Pei, S.P., 2002. Pn & Sn tomography of uppermost mantel in China. [Ph. D, thesis] (in Chinese). Institute of Geophysics, China Earthquake Administration, Beijing.

Pei, S.P., Xu, Z.H., Wang, S.Y., 2003. A review on refraction wave travel time tomography of uppermost mantle. Prog. Geophys. 18 (1), 59–64 (in Chinese with English abstract).

Pei, S.P., Zhao, J.M., Sun, Y.S., Xu, Z.H., Wang, S.Y., Liu, H.B., Rowe, C.A., Nafi Toksöz, M., Gao, X., 2007. Upper mantle seismic velocities and anisotropy in China determined through Pn and Sn tomography. J. Geophys. Res. 112, B05312. https://doi.org/10.1029/2006JB004409.

Ren, G.T., Yan, Y.F., 1987. A study about the relation between regional magnetic anomaly and crustal structure in Panxi region. Acta Geophys. Sin. 30 (6), 594–601 (in Chinese with English abstract).

Royden, L.H., Burchfiel, B.C., King, R.W., Wang, E., Chen, Z., Shen, F., Liu, Y., 1997. Surface deformation and lower crustal flow in eastern Tibet. Science 276 (5313), 788–790. https://doi.org/10.1126/science.276.5313.788.

Shi, Y.T., Gao, Y., Zhang, Y.J., 2013. Shear-wave splitting in the crust in eastern Songpan-Garze block, Sichuan-Yunnan block and western Sichuan basin. Chinese J. Geophys. 56 (2), 481–491 (in Chinese with English abstract).

Silver, P.G., Chan, W.W., 1988. Implications for continental structure and evolution from seismic anisotropy. Nature 335 (6185), 34–39. https://doi.org/10.1038/335034a0.

Silver, P.G., Chan, W.W., 1991. Shear wave splitting and subcontinental mantle deformation. J. Geophys. Res. 96 (B10), 16429. https://doi.org/10.1029/91jb00899.

Sun, W.J., Kennett, B.L.N., 2016. Uppermost mantle P wavespeed structure beneath eastern China and its surroundings. Tectonophysics 683, 12–26. https://doi.org/10.1016/j.tecto.2016.06.011.

Teng, J.W., Wang, F.Y., Zhao, W.Z., Zhang, Y.Q., Zhang, X.K., Yan, Y.F., Zhao, J.R., Li, M., Yang, H., Zhang, H.S., Ruan, X.M., 2010. Velocity structure of layered block and deep dynamic process in the lithosphere beneath the Yinshan orogenic belt and Ordos Basin. Chin. J. Geophys. 53 (1), 67–85 (in Chinese with English abstract).

Teng, J.W., Zhang, Z.J., Zhang, X.K., Wang, C.Y., Gao, R., Yang, B.J., Qiao, Y.H., Deng, Y.F., 2013. Investigation of the Moho discontinuity beneath the Chinese mainland using deep seismic sounding profiles. Tectonophysics 609, 212–216. https://doi.org/10.1016/j.tecto.2012.11.024.

Tian, X.B., Teng, J.W., Zhang, H.S., Zhang, Z.J., Zhang, Y.Q., Yang, H., Zhang, K.K., 2011. Structure of crust and upper mantle beneath the Ordos Block and the Yinshan Mountains revealed by receiver function analysis. Phys. Earth Planet. Inter. 184 (3), 186–193.

Wang, Q.S., Teng, J.W., Zhang, Y.Q., Zhang, X.M., Yang, H., 2009. The crustal structure and gravity isostasy in the middle western Sichuan area. Chinese J. Geophys. 52 (2), 579–583 (in Chinese with English abstract).

Wang, C.Y., Chan, W.W., Mooney, W.D., 2003a. Three-dimensional velocity structure of

crust and upper mantle in southwestern China and its tectonic implications. J. Geophys. Res. 108 (B9), 2442. https://doi.org/10.1029/2002JB001973.

Wang, H.Y., Hearn, T.M., Chen, Y.S., 2013a. Pn wave tomography of eastern Tibetan plateau. Chinese J. Geophys. 56 (2), 472–480 (in Chinese with English abstract).

Wang, X.B., Luo, W., Zhang, G., Cai, X.L., Tan, Q.Y., Luo, H.Z., 2013b. Electrical structure of Longmenshan crust-mantle under sector boundary. Chinese J. Geophys. 56 (8), 2718–2727 (in Chinese with English abstract).

Wang, Q.S., Teng, J.W., Zhang, Y.Q., Yang, H., 2008. The effect of crustal gravity isostasy and Wenchuan earthquake in Longmenshan faults and adjacent area. Prog. Geophys. 23 (6), 1664–1670 (in Chinese with English abstract).

Wang, S.Y., Xu, Z.H., Pei, S.P., 2003b. Pn velocity variation beneath China mainland and deep structure background for earthquake generation. Chinese J. Geophys. 46 (6), 779–785 (in Chinese with English abstract).

Wen, L.M., Badal, J., Hu, J.F., 2018. Anisotropic H-k stacking and (revisited) crustal structure in the southeastern margin of Tibet. J. Asian Earth Sci. 169, 93–104. https://doi.org/10.1016/j.jseaes.2018.07.028.

Wu, J.P., Ming, Y.H., Wang, C.Y., 2006. Regional waveform inversion for crustal and upper mantle velocity structure below Chuandian region. Chinese J. Geophys. 49 (5), 1369–1376 (in Chinese with English abstract).

Xiong, X.S., Gao, R., Zhang, J.S., Wang, H.Y., Guo, L.H., 2015. Differences of structure in mid-lower crust between the eastern and western blocks of the Sichuan basin. Chinese J. Geophys. 58(7), 2413–2423, 10.6038/cjg20150718 (in Chinese with English abstract).

Xu, L.L., Rondenay, S., Van der Hilst, R.D., 2007. Structure of the crust beneath the southeastern Tibetan Plateau from teleseismic receiver functions. Phys. Earth Planet. In. 165 (3–4), 176–193. https://doi.org/10.1016/j.pepi.2007.09.002.

Xu, Y., Li, Z.W., Huang, R.Q., 2010. Pn-wave velocity and anisotropy of the western Sichuan and Longmenshan Mountain region. China. Sci. China Seri. D, Earth Sci. 40 (4), 452–457 (in Chinese).

Yang, H., Teng, J.W., Wang, Q.S., Pi, J.L., 2013. Numerical simulation on the special gravity fields and dynamic response in Longmenshan orogenic belt and adjacent area. Chinese J. Geophys. 56 (1), 106–116 (in Chinese with English abstract).

Yang, Y., Liu, M., 2009. Crustal thickening and lateral extrusion during the Indo-Asian collision: a 3D viscous flow model. Tectonophysics 465 (1–4), 128–135. https://doi.org/10.1016/j.tecto.2008.11.002.

Yang, Z.X., Wang, F.Y., Duan, Y.H., Zhang, C.K., Zhao, J.R., Zhang, J.S., Liu, B.F., 2011. Basement structure of southeastern boundary region of Sichuan-Yunnan active block:

analysis result of Yanyuan-Xichang-Zhaojue-Mahu deep seismic sounding profile. Acta Seismol. Sin. 33 (4), 431–442 (in Chinese with English abstract).

Yao, Z.X., Wang, C.Y., Zeng, R.S., Lou, H., Zhou, M.D., 2014. Crustal structure in western Qinling tectonic belt and its adjacent regions deduced from receiver functions. Acta Seismol. Sin. 36 (1), 1–19. https://doi.org/10.3969/j.issn.0253-3782.2014.01.001 (in Chinese with English abstract).

Zhang, L.T., Jin, S., Wei, W.B., Ye, G.F., Duan, X.S., Dong, H., Zhang, F., Xie, C.L., 2012. Electrical structure of crust and upper mantle beneath the eastern margin of the Tibetan plateau and the Sichuan basin. Chinese J. Geophys. 55 (12), 4126–4137 (in Chinese with English abstract).

Zhang, P.Z., 2008. Current tectonic deformation, strain distribution and deep dynamic process of eastern margin of Qinghai-Tibet Plateau in western Sichuan. Sci. China, Earth Sci. 38 (9), 1041–1056.

Zhang, B.W., Zhao, C.P., Zhou, L.S., 2015a. Crustal thickness and poisson's ratio beneath the east boundary of Sichuan-Yunnan block from receiver functions. Earthquake 35 (1), 55–64 (in Chinese with English abstract).

Zhang, S.B., Zheng, Y.F., Wu, Y.B., Zhao, Z.F., Gao, S., Wu, F.Y., 2006. Zircon U-Pb age and Hf-O isotope evidence for Paleoproterozoic metamorphic event in South China. Precambr. Res. 151 (3–4), 265–288. https://doi.org/10.1016/j.precamres.2006.08.009.

Zhang, Y.Q., Mercier, J.L., Vergély, P., 1998. Extension in the graben systems around the Ordos (China), and its contribution to the extrusion tectonics of south China with respect to Gobi-Mongolia. Tectonophysics 285 (1–2), 41–75.

Zhang, G., Wang, X.B., Fang, H., Guo, Z.M., Zhang, Z.B., Luo, W., Cai, X.L., Li, J., Li, Z., Wu, X., 2015b. Crust and upper mantle electrical resistivity structure in the Panxi region of the eastern tibetan plateau and its significance. Acta Geol. Sin. – English Ed. 89 (2) 5 32–541.

Zhang, Y.Q., Wang, Q.S., Teng, J.W., 2010. The crustal isostatic anomaly beneath eastern Tibet and western Sichuan and its relationship with the distribution of earthquakes. Chinese J. Geophys. 53 (11), 2631–2638 (in Chinese with English abstract).

Zhang, Z.J., Teng, J.W., Romanelli, F., Braitenberg, C., Ding, Z.F., Zhang, X.M., Fang, L.H., Zhang, S.F., Wu, J.P., Deng, Y.F., Ma, T., Sun, R.M., Panza, G.F., 2014. Geophysical constraints on the link between cratonization and orogeny: evidence from the Tibetan Plateau and the North China Craton. Earth-Sci. Rev. 130, 1–48. https://doi.org/10.1016/j.earscirev.2013.12.005.

Zhou, Z.G., Lei, J.S., 2016. Pn anisotropic tomography and mantle dynamics beneath China. Phys. Earth Planet. In. 257, 193–204.